Makara Journal of Technology

Volume 26 | Issue 3 Article 3

12-30-2022

Design and Prototyping of a Low-Cost High Frequency Antenna for Vicinity Coupling Devices

Benjamin Kommey
Department of Computer Engineering, Faculty of Electrical and Computer Engineering, Kwame Nkrumah University of Science and Technology, Kumasi 00233, Ghana, bkommey.coe@knust.edu.gh

Ernest Ofosu Addo
Department of Computer Engineering, Faculty of Electrical and Computer Engineering, Kwame Nkrumah University of Science and Technology, Kumasi 00233, Ghana, erny.addo@gmail.com

Elvis Tamakloe
Department of Computer Engineering, Faculty of Electrical and Computer Engineering, Kwame Nkrumah University of Science and Technology, Kumasi 00233, Ghana, tamakloe.elvis@gmail.com

Makara J. Technol. 26/3 (2022), 103–109
doi: 10.7454/mst.v26i3.1564

Design and Prototyping of a Low-Cost High Frequency Antenna for Vicinity Coupling Devices

Benjamin Kommey*, Ernest Ofosu Addo, and Elvis Tamakloe

Department of Computer Engineering, Faculty of Electrical and Computer Engineering,
Kwame Nkrumah University of Science and Technology, Kumasi 00233, Ghana

*E-mail: bkommey.coe@knust.edu.gh

Abstract

This paper describes the development of a high frequency (HF) antenna for high output power vicinity coupling devices (VCDs) operating at 13.56 MHz. Key design parameters, such as RF power level, antenna size, and communication protocol, and their link to the antenna features and requirements, have been discussed. For efficient reader interrogation, detection, and recovery of transponder responses, a tuning circuit necessary to adjust the antenna power matching and resonance characteristics was designed and prototyped. The antenna was fed to an industry standard reader and evaluated for read range performance with vicinity cards. The designed antenna on the reader achieved a good read range, which demonstrated fair agreement with the calculated theoretical results.

Keywords: antenna, high frequency, RFID, tuning network, vicinity coupling devices

1. Introduction

Automatic identification procedures have become universal elements in many manufacturing, service, energy, and transportation industries [1], [2]. These procedures exist to satisfy the age-old need of providing information regarding people and goods in transit. Methods, such as bar-coded label reading and optical character recognition, are still popular due to their low prices. Thus, radio frequency identification (RFID) has garnered increasing interest since the turn of the century and its use has been forecasted to experience a large growth in this decade [3]. RFID offers a technically optimal solution to the problem of low data storage capacity and non-reprogrammable capability associated with the methods mentioned earlier. This technology also provides a fast, hard, and secure means of power and data transfer between a tag on a remote body to be identified and a reader or interrogator using magnetic or electromagnetic (EM) waves. Furthermore, the non-line-of-sight operation of RFID and its multiple object identification capabilities have made it widely preferred for use in inventory control and automation applications.

RFID systems exist in many variants and possess fundamental differentiating features. These systems may be classified on the basis of several factors, such as operation type, operating principle of the data carrier, power supply, operating frequency range, or mode of data transfer. An RFID transponder is considered passive if it does not have its power but draws power from the field launched by a reader. By contrast, active tags incorporate batteries to supply all or part of the power required for its operation. Based on the reader transmission frequency, RFID devices may be considered as follows: low frequency (30–300 kHz), high frequency (3–30 MHz), ultrahigh frequency (0.3–3 GHz), or microwave (>3 GHz) systems. The HF class of RFID devices generally operates at f_{op} = 13.56 MHz (wavelength, $\lambda_{op} \approx 22$ m) in the ISM band and can achieve a read range up to 1 m. These devices work based on a transformer type magnetic coupling principle illustrated in Figure 1. Herein, the power and data transfer between a reader and tag occurs inductively in the reactive near-field (enclosing sphere of radius $\frac{\lambda_{op}}{2\pi}$) of antennas of both devices. The operation of HF devices is regulated by various standards, which include the ISO 18000 set of general standards for RFID, ISO 14443, ISO 15693, and

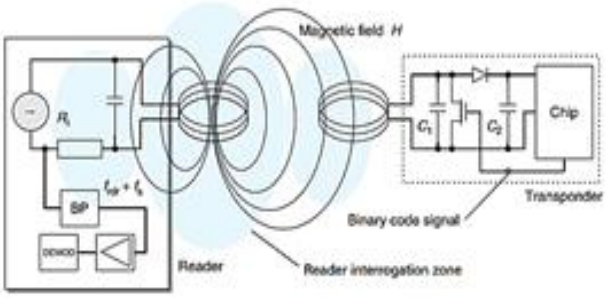

Figure 1. Schematic View of the Operation in HF-RFID Systems (Addo *et al.* [22])

the EPCglobal Class 1 Gen 2. The standards define key radio interface parameters, such as modulation, subcarrier frequency, bandwidth, and coding [4]. This paper focuses on HF-RFID devices that conform to the ISO 15693 standards, wherein tags are referred to as vicinity integrated circuit cards (VICCs) and vicinity coupling devices (VCDs) of readers. The challenge of signal reception and processing as experienced by many VICCs and readers in object identification cannot be overlooked.

Various attempts toward the development of antennas for such devices are detailed in the recent literature. The paper in [5] proposes a method for creating large area antenna structures for VCDs. In that paper, a four-element antenna was produced by marking conductive inks on a paper substrate using a stencil process. An input power of 33 dBm produced a maximum recorded read range of 11.1 cm using the tag antenna system. Thus, antennas produced from such a method suffered remarkably high losses and possessed poor power transfer to passive tags. The proposed remedy for this problem involves applying the conductive ink to an identical position multiple times, which significantly increases the fabrication complexity and system cost of such antennas. In [6], a multiloop antenna structure for use in an industrial setting was developed. A model where the antenna is divided into a few finite length elements to combat the effect of eddy currents produced in antennas by metallic objects in the antenna surroundings is presented in this paper. This model has a maximum recorded read range of 43 cm in disruption-free environment when the tag and reader are in close proximity at 94 dBμA/m magnetic field. The design approach in the paper produced antennas which worked well near conductive materials; however, these antennas could not read mid-range tags well and were only useful for low read distance applications, such as smart shelving. The authors in [7] presented a model for developing HF-RFID antennas based on the idea of using the self-resonance frequency of small multi-turn coils. Their model sought to optimize the quality factor and provide uniform near-field patterns. However, the approach required intricate printed circuit board (PCB) technology, produced substantially low read distances with a maximum value of 10 cm, and relied on special substrates for a decent performance.

The current work presents a methodical design of a low fabrication cost RFID antenna, which guarantees a good detection range and an easy recovery of responses from VICCs present in the interrogation zone of the reader. The main contribution of the paper is to demonstrate the implementation of an HF antenna for VCDs, which uses a low-cost and less complex construction approach yet provides a superior performance compared with the recent state-of-the-art. An antenna prototype was developed and tested to validate the proposed method.

2. Materials and Methods

Design considerations. Based on their principle of operation, antennas for HF-RFID applications are designed as electrically small loops. Loop antennas can be designed for appreciable self-inductance required for tag–reader inductive coupling. Antennas could be made from any conductive material, with copper and aluminum being the common materials. Construction methods include the use of tubes and tapes [8–9], wire (insulated or non-insulated) [10], PCB etching [7, 11, 12], and screen printing [5, 13].

Tube antennas are often bulky despite their easy production, while tape antennas lack robustness because they easily succumb to environmental conditions. PCB antennas are neat and are suitable for miniature systems. Such antennas might not necessarily require industry-grade equipment nor processes and can be created by an average skilled handyman. However, etching PCB antennas involves the use of harmful materials, such as ferric chloride acid. Hence, the manufacturing process should be performed meticulously and with safety equipment. Antenna coils could also be realized by screen printing with conductive inks (e.g., silver particle ink) on various substrates, such as paper or PET. Despite the remarkable design flexibility and low-cost advantages of this technique, screen printed antennas have high fabrication complexity. Additionally, these printed antennas are plagued with reduced read performance (low quality factor and low signal-to-noise ratio) and high Joule heating due to their commonly high DC resistance [14–15]. Wire antennas provide a good balance of the aforementioned pros and cons and are considered in this work.

Knowledge of the overall RFID system features, such as the VCD, RF supply, and possible VICC characteristics, is crucial to obtain the optimum performance of the antenna. VCDs require antennas with their center frequency tuned to f_{op} and having an input impedance that matches the interrogator front-end/supply with minimal small reflection loss. The VCD must also possess good tag response selectivity when the designed antenna is connected. Another important influence on the design is the required maximum reading range d_{max}. For a given VCD RF output power, the read distance bears a strong dependence on the size of the reader antenna. Considering a square HF loop antenna fed with current I, provided the total loop conductor length $D << 0.2\lambda_{op}$, the magnetic field intensity at a distance d along the normal axis of the loop could be accurately estimated using Equation (1), where N and s are the turns number and side dimension of the antenna, respectively [16].

$$H(d) \approx \frac{2\sqrt{2}NIs^2}{\pi\sqrt{(2d^2+s^2)^3}} \quad (1)$$

Among all shapes of similar perimeter, the antenna coil was designed in a square shape because it produces the largest near-field magnetic field required for VCD–VICC communication [20]. This shape is commonly used because it is quite simple to construct and performs better in practice compared with other shapes. Furthermore, Equation (1) shows that long read ranges are guaranteed by large power. However, the RF power or field generated by an antenna has a legal limit, which is 4 W in Europe and the USA based on ETSI and FCC regulations, respectively [8]. Large antennas may require shielding to maintain their operation within these limits. The adoption of large loops could also negatively affect the receiving characteristics of the antenna and increase coil self-inductance to levels which may make power matching remarkably difficult to achieve. Other factors, such as typical tag traveling speed, orientation, and transmitted data volume, are also considered in the system requirement study [6]. The effect on travel speed and data transmission, which are remarkably critical in simultaneous multiple tag identification, could be linked to the VCD, baud rate, and sojourn time of tags in the field.

Antenna design. In the reactive near-field region of the square loop antenna, the power is predominantly inductive and tends to be real as *d* increases. Therefore, the square loop could be equivalently represented by a series *RL* lumped element connection; with distributed capacitance *coil* between coil turns, the antenna exhibits bandpass filtering properties. At f_{op} and with a core of magnetic permeability μ, an *s*-side square loop antenna constructed from *N* turns of a conductor of diameter *h* and conductivity σ presents an input resistance R_{coil}, which combines its radiation resistance R_{rad} and ohmic resistance R_{loss} Equation (2). Additionally, the antenna exhibits a self-inductance L_{coil} that could be evaluated by the expression in Equation (3) [17].

$$R_{coil} \approx 20\pi^2 N^2 \left(\frac{4s}{\lambda_{op}}\right)^4 + \frac{4Ns}{h}\sqrt{\frac{f_{op}\mu}{\pi\sigma}}, \quad (2)$$

$$L_{coil} \approx 2N^2 s \frac{\mu}{\pi}\left(\frac{2a}{h}\right) - 0.774. \quad (3)$$

Antenna turning network Q-Damping. In VICC-to-VCD communication, the modulated tag response is captured by the antenna of VCD and relayed to its receiver front-end for demodulation. The received signal is directly downconverted, amplified, and bandpass filtered to remove DC and high-order conversion components, extracting only the frequency band holding the subcarrier signal, that is, the sidebands of the received signal spectrum.

A large quality factor $Q = \frac{f_{op}}{BW_{3dB}}$ indicates high output power for the antenna but narrow half-power bandwidth, *BW3dB,* and possible stability issues. Therefore, the design of the reader antenna *Q* involves a compromise between large d_{max} and good carrier–subcarrier separation. A high *Q* may conflict with the bandpass response of the reader, and increased signal oscillations could interfere with the protocol parameters of VCD, such as bit timing [18–19]. Furthermore, high voltages at resonance can cause insulation breakdown of the coil or conditioning circuit components depending on the antenna build. The antenna must be damped to mitigate such problems. That is, the interrogator antenna must be designed such that it has sufficient bandwidth for the undistorted transmission or reception of a modulated carrier signal while having sufficient power to meet the minimum interrogation field strength (H_{min} criterion of VICCs). Typical values for VICC interrogation *H* range from 0.075 A/m to 5 A/m. As recommended in the ISO 15693 standard, the loaded VCD antenna *Q*, Q_L, must lie in the range of 15–20 for good performance (Figure 2) [5, 8].

Assuming C_{coil} is remarkably small at f_{op}, the antenna is approximately a first-order series resonator with a large time constant $\tau = \frac{L_{coil}}{R_{coil}}$. Therefore, the unloaded quality factor of the antenna, $Q_{0,}$ is given by Equation (4). The high unloaded *Q* (due to the large τ) could be lowered to a recommended overall value, Q_L, by loading the antenna with a large shunt resistance R_{par} to produce an effective anti-resonance with a low-quality factor.

$$Q_{ext} = \frac{R_{par}}{\omega_{op} L_{coil}}, \text{ Since } R_{par} >> R_{coi,}$$

$$Q_L = Q_0 || Q_{ext} \approx Q_{ext}.$$

Therefore, in designing the damping network, a desired Q_L is first selected, and the appropriate shunt resistor value can be determined as $R_{par} \approx \omega_{op} L_{coil} Q_L$. This resistance value could be fine-tuned for optimum performance.

$$Q_0 = 2\pi f_{op}\tau = \frac{\omega_{op} L_{coil}}{R_{coil}}. \quad (4)$$

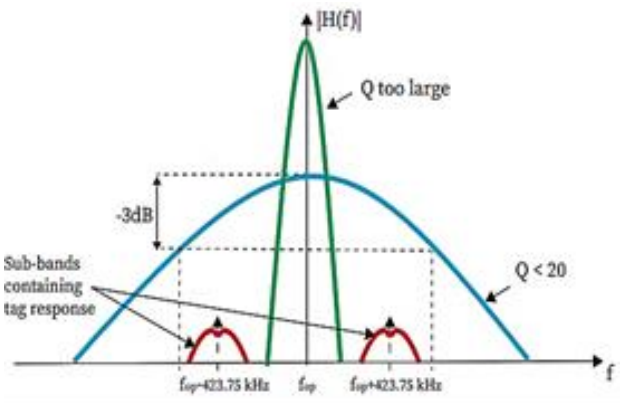

Figure 2. Antenna Bandpass Characteristics with Low and High Q (Addo *et al*. [22])

Impedance matching and resonance. At HF frequencies, RF voltage can no longer be considered stationary but must be treated as an EM wave in the supply cable. Therefore, a 50Ω coaxial or shielded cable is commonly used to feed the antenna coil to prevent undesired standing-wave phenomena, such as parasitic power emissions and signal reflections. Z_{coil} must be transformed to the feed resistance R_X = 50Ω using a passive matching circuit as shown in Figure 3 to achieve power matching between the antenna and the reader output module via the coax supply. Furthermore, the tuning network should feature a capacitance $C_{par} = \frac{1}{\omega_{op}^2 L_{coil}}$, which brings the antenna to resonance at f_{op} when shunted across the coil. The peaking of voltage at f_{op} for a given L_{coil} increases the generated magnetic flux required to supply power to the tag for reading, writing, or locking operations. Therefore, the performance of this resonant circuit influences the read range of the reader system. Additionally, an excellent power matching translates to the large energy available for flux generation.

A practical configuration of capacitance matching is shown in Figure 5. In this matching circuit, the shunt C_{par} is split into series and parallel capacitance elements C_1 and C_2, each satisfying the resonance and input impedance matching conditions, respectively. C_1 shifts the damped antenna impedance $Z_{coil}' = Z_{coil}||R_{par}$ in the direction of the jX axis shown in Figure 4, while C_2 shifts the Z_{coil}' away from the origin in a circular path in the Z-plane [20]. The splitting of C_{par} into C1 and C_2 introduces an additional degree of freedom to the matching network design [10]. A simplified dimensioning of C_2 and C_1 from C_{par}, R_{par}, and R_X is approximated in Equations (5) and (6), respectively. The obtained values of C_2 and C_1 are inexact and may need tuning. The circuit is then refined to function as a balun to eliminate effects, such as common mode noise, ringing, or unwanted coax radiation. These effects may arise due to the high (AC) voltage difference between the coax core and the grounded outer shield. Figure 5 shows the balanced capacitance matching circuit.

$$C_2 \approx C_{par}\sqrt{\frac{R_{par}}{R_x}}, \quad (5)$$

$$C_1 = \frac{C_2 C_{par}}{C_2 - C_{par}}. \quad (6)$$

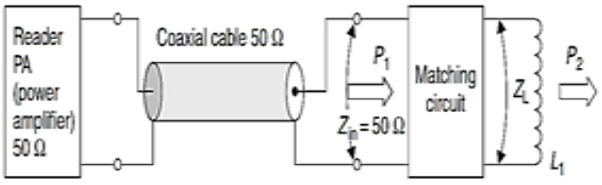

Figure 3. Connection of an Antenna Coil to a VCD via 50Ω Technology

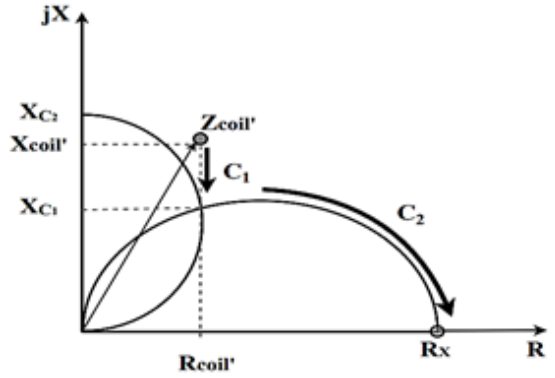

Figure 4. Transformation of Zcoil′ by C1 to C2 is Represented in the Z-plane (Addo *et al.* [22])

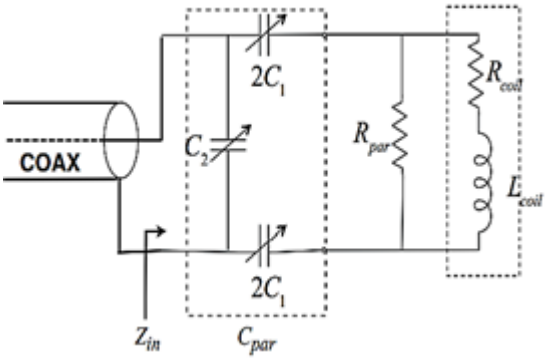

Figure 5. Circuit of Antenna Coil with a Balanced Capacitance Matching Network (Addo *et al.* [22])

3. Prototyping of Antenna

A single-turn square loop HF antenna with 40 cm side dimensions was designed to operate at f_{op}, simulated, and realized from a copper wire with 1 mm diameter. From Equations (2) and (3) with $\sigma_{Cu} = 5.8 \times 10^7$ S/m and $\mu = \mu_0 = 4\pi \times 10^{-7}$ H/m, R_{coil} and L_{coil} were computed as 0.495Ω and 1.891 μH, respectively. Therefore, the calculated impedance of the square loop antenna was Z_{coil} = 0.495 + j161.45Ω. The analytical derivation of the antenna input impedance was validated using CST Microwave Studio. The simulated antenna model presented in Figure 6 has an input impedance of 0.506 + j164.44Ω. The simulated and computed Z_{coil} are in good agreement. The antenna was fabricated by molding the copper wire into a 40 cm side square loop and affixing it to cardboard. The loop was then fitted with a terminal block receptacle for easy connection (disconnection) to the (from) the antenna tuning network. The input impedance of the realized antenna was determined by measuring the complex power reflection coefficient S_{11} at the antenna port using an Agilent E5071c vector network analyzer (VNA) via a terminal block-to-coax connector and coaxial cable. The antenna prototype is shown in Figure 7. The measured input impedance of the

antenna at f_{op} was $Z_{coilM} = R_{coilM} + jX_{coilM} = 2.187 + j191.282\Omega$. Therefore, the measured input resistance and self-inductance of the antenna were $R_{coilM} = 2.187\Omega$ and $L_{coil_M} = \frac{X_{coil_M}}{\omega_{op}} = 2.245\mu H$, respectively. The increase or deviation of the measured input impedance considering the analytical and simulated values could be mainly attributed to the increase in D and s due to error during prototyping Equation (2) and (3). For R_{ecoil}, although R_{ead} has a quartic dependence on s, the $1/t_{op}$ multiplicative factor diminishes the effect of increasing s because $s < a < t_{op}$. Thus, the increment in R_{ecoil} mainly corresponds to the osmic loss increase. However, the operation of HF-RFID antennas does not depend on R_{ead} because such systems rely solely on inductive power. By contrast, the increase in L_{ocal} is attributed to the rise of the unloaded Q of the antenna coil $Q_0 \approx 87$ (Equation (4)) due to$s$ $\ln\left(\frac{2s}{h}\right)$, which was more than four times the recommended limit. Designing for a Q_L =17, a shunt resistor $R_{ap} = \omega_{op}L_{coilM}Q_L = 3.25k\Omega$ was used as an initial guess. This resistance value was tuned later for optimum performance. The capacitance matching technique was used to transform the damped antenna impedance to R_X. The resonance capacitance C_{par} was determined to be = $\frac{1}{\omega_{op}{}^2 L_{coil_M}} = 61.36$ pF, whiles C_1 and C_2 were 70 and 495 pF (Equations (5) and (6), respectively). The circuit representation of the reader antenna connected to a balanced capacitance matching network was simulated and tuned in the NI AWR Design Environment. The optimized damping and matching circuit parameter values were $R_{par} = 3.266k\Omega$, $C_1 = 70$pF, and $C_2 = 384$pF (Figure 8). As shown in the plot in Figure 9, the optimized balanced matching circuit resonates at 13.82 MHz and has an input impedance $Z_{in} = 50.04 - j0.0768\Omega$ at f_{op}. The antenna achieved a simulated 68.17 dB return loss at its input port when connected to the 50Ω port (coax supply).

The matching network was fabricated on an FR-4 PCB with etched copper traces for the easy connection of circuit components. The PCB was fitted with a terminal mounting header and an SMA Female PCB Edge Mount

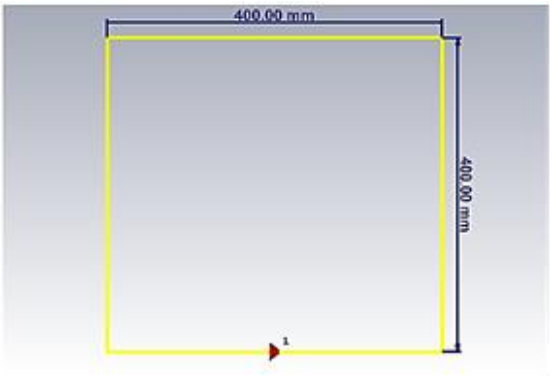

Figure 6. 3D Model of the Antenna

for connecting the circuit to the antenna and the reader supply, respectively. SMD resistors and capacitors as well as the connectors were soldered to the copper traces to complete the matching circuit. R_{par}, C_1, and C_2 were formed with a combination of low-valued devices due to the unavailability of exact valued discrete components.

The component part list is summarized in Table 1 and Figure 10 shows the fabricated matching circuit.

The antenna matching circuit assembly was measured using the VNA and then tuned for optimal matching at f_{op}. The measurement setup is shown in Figure 11.

Figure 7. Prototype of the Designed HF Antenna

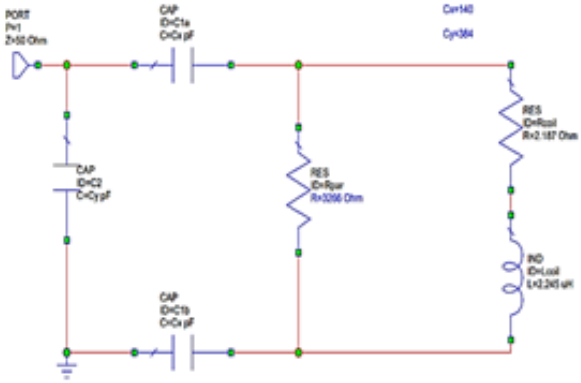

Figure 8. Schematic of HF Antenna with the Simulated and Optimized Balanced Matching Circuit

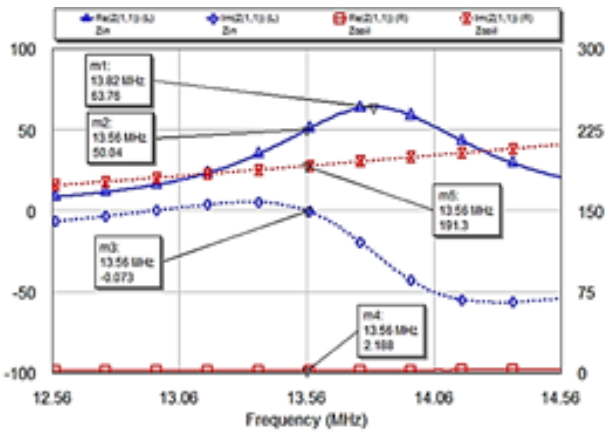

Figure 9. Impedance Plot of Z_{in} and Z_{coil} Over a 2 MHz Band Centered at f_{op}

Table 1. Bill of Material for the Matching

Circuit Elements	Optimal Value	Part Number	Part Value	Quantity
R_{par}	3.266 kΩ	RS 123-4452	3.3 kΩ	1
C_1	70 pF	RS 774-0594	100 pF	2
		RS 106-2893	7–50 pF	2
		RS 699-8666	220 pF	1
C_2	384 pF	RS 916-3056	150 pF	1
		RS 721-5350	6.5–30 pF	1

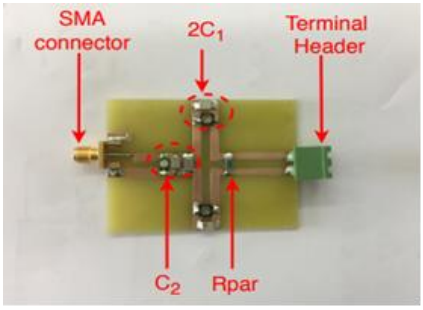

Figure 10. Prototype of the Balanced Damping and Matching Circuit

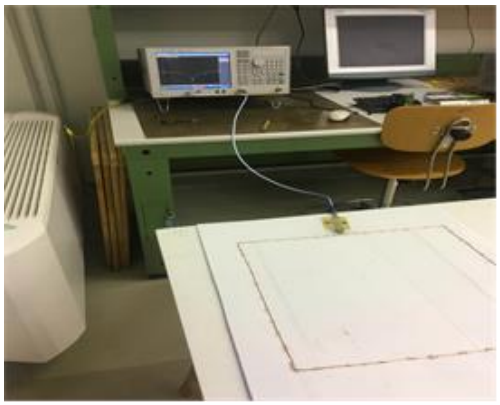

Figure 11. Measurement and Tuning of Antenna Port Matching Level

4. Results and Discussion

Read range measurements were conducted to test the performance of the VCD antenna. The antenna assembly was affixed to a wooden stand and fed by an OBID i-scan® HF long-range reader via a 50Ω coaxial line. The reader hardware was connected serially (via RS232 interface) to a measurement software (ID ISOStart software) on a computer. The measurement setup is shown in Figure 12.

The RF energy supply of the VCD was activated, and the noise floor was measured to ensure that the amplitude of interference level was sufficiently low such that tag responses could easily be identified even at low signal levels. A low noise floor was also an indication of a good antenna matching circuit and test environment setup. Differences in maximum and minimum noise levels should be less than 20 mV for good reader–tag communication. The average noise level recorded was 6 mV, while differences between extreme levels were 5 mV. Notably, in addition to the losses due to mismatch between the cable and the antenna, the reader also drives varied output currents depending on the antenna impedance, resulting in power variance [21]. A 50 Ω load draws approximately 0.3 A of current. No current flows when the output is open, and the current is limited to 1.0 A in the event of a short circuit.

The read range of three NXP VICCs (H_{min} = 0.09A/m) was tested. Each card was positioned at the center of and in parallel with the reader antenna plane. Assuming perfect matching at the reader and antenna ports, for the single-turn s^2 square loop reader antenna, the maximum theoretical read range of the HF-RFID system with a parallel tag is given by Equation (7). The distance between each card and the reader antenna fixture was increased until the magnetic coupling between the two units was severed and the card reading was lost. The longest recorded read range was 0.48 m. The measured range demonstrated fair agreement with the results obtained in Equation (7). Table 2 summarizes the properties and read range performance of the presented design compared with the recent state-of-the-art implementation of HF antennas for VCDs.

$$d_{max} \approx \sqrt{\left(\frac{NIs^2}{\pi H_{minNXP}}\right)^{\frac{2}{3}} - \left(\frac{s}{2}\right)^2} \approx 0.52m \qquad (7)$$

The measurement of the S parameter over a 2 MHz band as depicted in Figure 13 provides a typical overview of the prototype antenna performance.

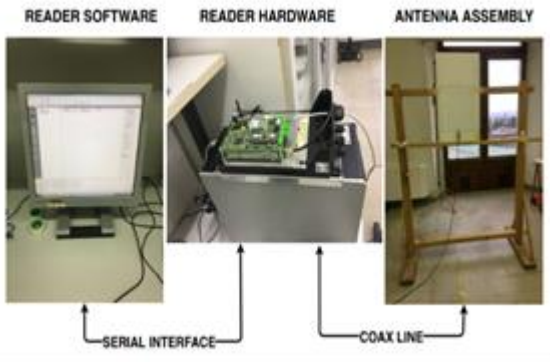

Figure 12. Read Range Measurement Setup (Addo *et al.* [22])

Table 2. Comparison of the Presented Work to the State-of-the Art

	Li *et al* [5]	Soheyl *et al.* [7]	Petrariu *et al.* [6]	This Work
Construction	Printed paper	PCB	Insulated wire	Bare wire
Material	Silver ink	Copper	Copper	Copper
Loop Geometry	Square	Circular	Rectangular	Square
Perimeter (m)	0.5	0.57	1.08	1.6
Number of Turns	4	2	2	1
Fabrication Complexity	High	Medium	Low	Very low
Read Range (m)	0.11	0.1	0.43	0.48

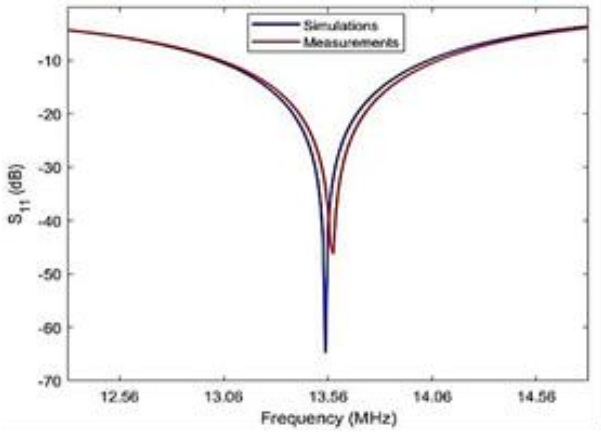

Figure 13. S11 Measurement Result of the Antenna

At 13.56 MHz operating frequency, a value of −68.17 dB was obtained from the simulation. Furthermore, −48.82 dB was measured at 13.60 MHz with the antenna prototype. Thus, the appreciable change in return loss was attributed to fabrication tolerances and measurement imperfections.

5. Conclusions

The design and prototyping of a square loop antenna for a 13.56 MHz VCD has been described in this paper. The design of a balanced damping and matching circuit required to adjust the input impedance, resonance, and quality factor of the antenna has been outlined. The matching circuit was optimized, fabricated, and connected to the antenna using a 50Ω technology feed. The antenna assembly was tuned, fed using an industry standard ISO 15963 compliant reader, and tested for read performance on vicinity cards. The designed antenna with the reader achieved a good read range, which demonstrated fair agreement with the calculated theoretical maximum read range. Compared with recent state-of-the-art implementations, the antenna presented in this work produces superior read performance while using a simple construction approach.

References

[1] M. Weglarski, P. Jankowski-Mihulowicz, M. Chamera, J. Dziedzic, P. Kwasnicki, Micromachines. 11/4 (2020) 420.
[2] A. Toccafondi, C.D. Giovampaola, F. Mariottini, A. Cucini, Appl. Comput. Electromagn. Soc. J. 25/6 (2009) 543.
[3] R. Das, RFID Forecasts, Players and Opportunities 2019–2029, IDTechEx, 2019.
[4] B. Dakic, M. Damnjanovic, L. Zivanov, A. Menicanin, N. Blaz, M. Kisic, IEEE Jubilee Int. Symp. Intell. Syst. Informatics. (2012) 429.
[5] X. Li, J. Siden, H. Andersson, T.R. Schoen, IEEE J. Radio Freq. Identif. 2/3 (2019) 118.
[6] A. Petrariu, A. Lavric, E. Coca, Adv. Electr. Comput. Eng. 18/2 (2018) 35.
[7] S. Soheyl, T. Brown, AEU–Int. J. Electron. Commun. 78 (2017) 32.
[8] Texas Instruments, HF Antenna Design Notes Technical Application Report, Amerika, 2015.
[9] I. Kirschenbaum, A. Wool. Proc. USENIX Secur. Symp. (2006) 43.
[10] W. Aert, E. De Mulder, B. Preneel, G.A.E. Vandenbosch, I. Verbauwhede, IEEE Trans. Antennas Propag. 56/12 (2008) 3829.
[11] R. Jacobi, E. Lacost, Antenna Design Guide for the TRF79xxA Application Report, SLOA241C, Texas Instruments, Amerika, 2020.
[12] A.L. Borja, A. Belenguer, J. Cascon, R.J. Kelly, IEEE Antennas Wirel. Propag. Lett. 11 (2012) 580.
[13] G.G. Xiao, Z. Zhang, S. Lang, Y. Tao, Int. Symp. Antenna Technol. Appl. Electromagn. (2016) 1.
[14] G. Xiao, P. Aflaki, S. Lang, Z. Zhang, Y. Tao, C. Py, P. Lu, C. Martin, S. Change. IEEE J. Radio Freq. Identif. 2/1 (2018) 31.
[15] A. Koptioug, P. Jonsson, J. Siden, T. Olsson, M. Gulliksson, Antennas, (2003) 3.
[16] Y. Lee. Microchip Technol. Inc. (2003) 1.
[17] C.A. Balanis, Antenna theory: Analysis and design, Wiley-Interscience, New York, 2005, p.1104.
[18] X. Qing, Z.N. Chen, IEEE Antennas Propag. Mag. 51/2 (2009) 26.
[19] G. Xiao, Z. Zhang, H. Fukutani, Y. Tao, IEEE J. Radio Freq. Identif. 2 (2018) 111.
[20] K. Finkenzeller (Ed.), RFID handbook: fundamentals and applications in contractless smart cards, radio frequency identification and near field communication, 3rd ed., Wiley Publishing, New York, 2010, 480.
[21] FEIG Electronics, HF Loop Antenna, ID ISC.ANT310/310, Amerika Serikat, 2019.
[22] E.O. Addo, B. Kommey, A.S. Agbemenu, H. Kumbong, Eng. Rep. 3/10 (2020) e12407.